Spinodal decomposition in a lattice-gas automaton

Daniel H. Rothman, Stéphane Zaleski

Tome 50 N° 16 15 AOÛT 1989

LE JOURNAL DE PHYSIQUE

J. Phys. France **50** (1989) 2161-2174 15 AOÛT **1989,** PAGE 2161

Classification
Physics Abstracts
05.50+q — 64.75+g — 05.70Fh — 64.60Ht

Spinodal decomposition in a lattice-gas automaton

Daniel H. Rothman ([1]) and Stéphane Zaleski ([2])

([1]) Department of Earth, Atmospheric, and Planetary Sciences, Massachusetts Institute of Technology, Cambridge, Massachusetts 02139, U.S.A.
([2]) Laboratoire de Physique Statistique, CNRS, Ecole Normale Supérieure, 24 rue Lhomond, 75231 Paris Cedex 05, France

(*Reçu le 21 mars 1989, accepté le 5 mai 1989*)

Résumé. — Nous analysons un modèle de décomposition spinodale récemment introduit par Rothman et Keller. Ce gaz sur réseau immiscible a la particularité intéressante non seulement de conserver le nombre de particules et l'impulsion mais aussi de permettre des simulations hydrodynamiques avec interfaces mobiles. Nous présentons une étude expérimentale et théorique du comportement statistique du gaz sur réseau immiscible. Nous obtenons tout d'abord une estimation théorique du coefficient de diffusion en résolvant une équation de Boltzmann discrète. Les simulations numériques de la diffusion des particules d'une part et de la croissance des domaines d'autre part permettent de trouver la ligne spinodale du gaz sur réseau immiscible. Cette dernière est proche de la ligne où le coefficient de diffusion calculé théoriquement s'annule. Le gaz sur réseau immiscible constitue en outre un exemple intéressant de système où la dynamique microscopique est irréversible.

Abstract. — We analyze a lattice-gas model of spinodal decomposition recently introduced by Rothman and Keller. This immiscible lattice gas (ILG) is of special interest because it not only conserves momentum and particle number, but is also capable of hydrodynamic simulations of interfaces. Here we perform a jointly theoretical and empirical study of the statistical behavior of the ILG. We first obtain a theoretical prediction of the diffusion coefficient by solving a discrete Boltzmann equation. We then confirm, by numerical simulations of diffusion and domain growth kinetics, that the spinodal curve of the ILG is approximately given by the line in the space of density and concentration where the theoretical diffusion coefficient vanishes. The ILG is also an interesting example of a system with irreversible microdynamics.

Introduction.

There is a great interest in finding simple models of fluid mixtures on both the microscopic and macroscopic scales. On the microscopic level much is still to be learned about the

spinodal decomposition that leads to the separation of phases [1], as well as about the structure of interfaces themselves [2]. On the macroscopic level, the behavior of multiphase flows is extremely difficult to describe. These flows posses a rich phenomenology and are of industrial as well as fundamental interest.

Some progress may be expected with the help of a lattice-gas automaton (LGA) approach to the problem of fluid mixtures [3, 4]. In a lattice gas, fictitious particles hop from site to site on a regular lattice. When particles meet at a site, they undergo a simple, deterministic collision that conserves momentum and particle number. The large-scale behavior of LGA can be shown to obey the incompressible Navier Stokes equations [4] ; thus LGA offer an attractive alternative for the numerical simulation of hydrodynamics.

The phenomena observed in lattice gases are considerably enriched when LGA are extended to deal with mixtures of several species of particles [5]. When certain nearest-neighbor interactions are added, a surprising result is that a spinodal decomposition spontaneously occurs at a critical density [6]. A recent example of such a decomposition is illustrated in figure 1 [7]. Studies performed thus far indicate that such a model simulates immiscible fluid dynamics very similar to the dynamics of Newtonian fluids. Each of the pure phases behaves as the hexagonal lattice gases now well understood by researchers [4, 8, 9], while surface tension exists at the interfaces between phases. Since the behavior of this gas at sufficiently high densities is identical to that of a mixture of immiscible fluids, it is appropriate to label such LGA mixtures « immiscible lattice gases » (ILG's).

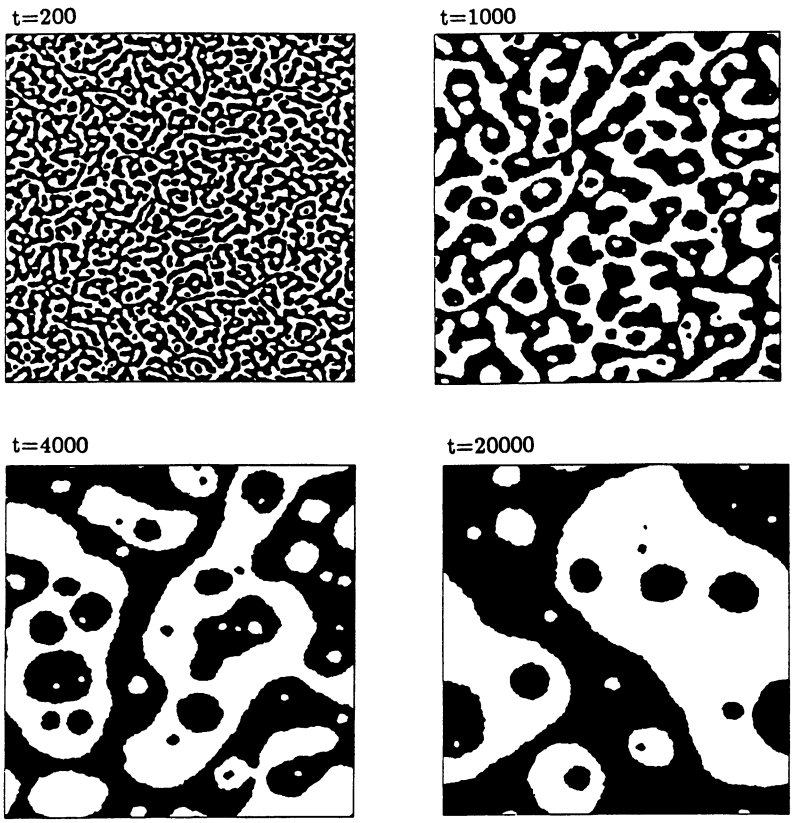

Fig. 1. — Spinodal decomposition in an immiscible lattice gas, on a 512×512 hexagonal lattice. Boundaries are periodic in both directions. From reference [7].

ILG's have already shown promise in a variety of different applications [10]. Our purpose in this paper, however, is to gain a fundamental understanding of the model. In particular, we study specific statistical properties of ILG's. This is not an easy task because of the peculiar nature of the statistical mechanics involved.

Unlike ILG's, most models of spinodal decomposition conserve an energy functional during their evolution. For example, Ising-like models conserve an energy of the form

$$H = -J \sum_{\langle i,j \rangle} s_i s_j + E \,, \tag{1}$$

where E is the energy of a heat bath at temperature T, J is a coupling constant, s_i is $+1$ if a site is « red » and -1 if a site is « blue », and $\langle i, j \rangle$ denotes nearest-neighbor sites. These models attempt to mimic closely the classical systems of statistical mechanics ; they are simulated either by Monte Carlo methods or by an explicit representation in cellular-automaton (also called microcanonical) models. The interaction energy common to these models favors the separation of the system into two phases when J/T is large enough. ILG models, however, are qualitatively different : there are interactions between nearest-neighbor sites but no energy is conserved. Thus, using standard arguments, one would not expect to see separation in ILG's because a separated state would be infinitely less likely than a mixed one ; i.e., the mixed state would win because it has higher entropy. How, then, may separation occur in the ILG, where interaction energy is absent ? The answer lies in the irreversible microscopic dynamics of the ILG. Because these dynamics are peculiar, fundamental principles of statistical mechanics, such as the existence of Gibbs states [11], may not hold. However, what is remarkable — and essential for applications — is that on the macroscopic scale not much difference is observed with real systems [6, 10].

The questions we thus seek to address are the following : what is the nature of the statistical state observed in the ILG ? How does it differ and how is it similar to classical systems of statistical mechanics ? Would an observer limited to the observation of macroscopic properties of the system such as density, momentum, etc., notice any difference ? For practical applications we obviously hope there is little difference but no theoretical justification is yet available.

Before we address such questions we find it useful to recall how separation of a mixture can be analyzed in the real world [1] (see Fig. 2). Separation occurs when the free energy of the system $F = U - TS$ (U is internal energy, S is entropy) has a minimum for two separated phases. Let a system of volume V be initially one mostly red phase, where x represents the fraction of reds, $0 \leqslant x \leqslant 1$, and $F(x, T, V)$ is the corresponding free energy. Assume the system separates into two homogeneous phases with red fractions x_1 and x_2, the first phase corresponding to a fraction α of the total number of particles. Then $x = \alpha x_1 + (1 - \alpha) x_2$ and the new free energy is $\alpha F(x_1) + (1 - \alpha) F(x_2)$. The condition for the stability of the initial phase of composition x is thus

$$F(x) \leqslant \alpha F(x_1) + (1 - \alpha) F(x_2) \,. \tag{2}$$

This condition will be verified for all x_1, x_2 and x if the function F is convex, i.e., if its second derivative is non-negative. The spinodal line is then the line in the T, x diagram on which the second derivative of the free energy is zero.

The unstable region inside the spinodal curve is a region where a system of composition x will spontaneously separate into two phases of neighboring compositions $x_1 \approx x \approx x_2$. There are also metastable states outside the spinodal which are unstable to nucleation of a phase of different composition x_2, with x_2 in the other well of figure 2. Because of surface tension, such a large change may occur very slowly : it is well known, for example, that superheated water

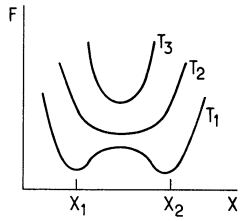

Fig. 2.

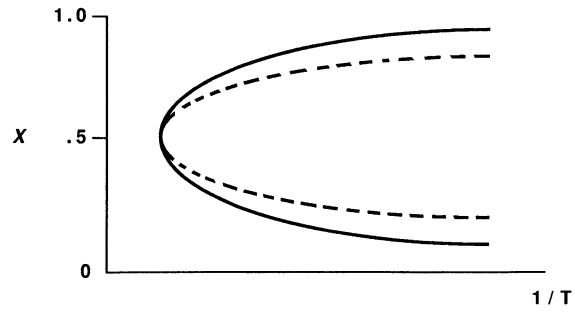

Fig. 3.

Fig. 2. — Typical free energy curves, for temperatures $T_1 < T_2 < T_3$. At T_3, the mixed phase is stable. T_2 is the critical temperature, below which the mixed phase is unstable.

Fig. 3. — Typical coexistence (solid) and spinodal curves (dashed).

may be metastable unless vapor bubbles of sufficient size are nucleated. Such metastable states are located between the minima of F and the spinodal. The minima of F thus delineate the « coexistence curve » of the mixture. Two phases may coexist in the system only if they are located on such points. When the two minima of the free energy merge the second derivative vanishes. Thus the coexistence and spinodal curves must meet on a critical line in a T, x phase diagram, as seen in figure 3. When a system passes through this critical line it undergoes a second-order phase transition.

Spinodal curves and coexistence curves may also be defined for the ILG. The relevant thermodynamic variables are now x and d, the reduced density (defined below) of the lattice gas. For example, a spinodal curve may be defined by observing where, in the x, d diagram, phases spontaneously decompose. A coexistence curve may also be determined by observing at which fractions x two phases may coexist.

In this paper we will be concerned exclusively with the prediction and measurement of the spinodal curve of the ILG. The prediction is made by assuming that the mixed phase is close to a factorized state, i.e., a state without correlation between sites. Although this assumption is a gross approximation, it becomes accurate in the limit of a vanishing density d. Importantly, it allows us to compute a diffusion coefficient, D, for the ILG. We then predict the spinodal curve by noting that the decomposition occurs when D becomes negative.

In what follows we shall first review the salient aspects of the ILG. We then define a Boltzmann equation for the ILG and solve it using a Chapman-Enskog expansion. The theoretical prediction of the diffusion coefficient is then compared with empirical estimates from numerical experiments. Knowledge of D allows the prediction of the spinodal curve. The theoretical spinodal curve is then compared with further empirical results obtained from numerical studies of domain growth.

Immiscible lattice gases.

The ILG model of reference [6] involves two types of particles — « red » and « blue » — living on a hexagonal lattice. We shall keep notations as close as possible to [4]. The velocities at a site are numbered from 0 to 6 with $\mathbf{c}_0 = 0$ and $\mathbf{c}_{j+1} = (\cos(2j\pi/6), \sin(2j\pi/6))$. The configuration of any given site is represented by 14 boolean variables r_i, b_i for $0 \leqslant i \leqslant 6$. r_i represents a red particle in direction i and b_i represents a blue particle, and there is at most one particle of each velocity. The configuration of a site is noted s where $s = (r_0, b_0, \ldots, r_6, b_6)$.

The lattice gas evolves in two steps. First, particles propagate to the nearest-neighbor sites at velocity $\mathbf{c}_i$. In the collision step care is taken to conserve the number of red and blue particles as well as the momentum. This creates 4 invariant quantities. The output configuration chosen will also depend on the nearest neighbors. To simulate attraction between particles of like color, those collisions which send red particles in the direction where the neighbors contain a relative majority of red particles should be favored, while blue particles should be sent towards neighboring blue particles.

The precise rules can be expressed in the following way. The configuration of a nearest neighbor in direction j is written $s^j = (r_0^j, b_0^j, \ldots, r_6^j, b_6^j)$. We also write $s_i = r_i + b_i$ and $s_i^j = r_i^j + b_i^j$. The configurations of all six neighbors can be represented as $\sigma = (s^1, \ldots, s^6)$. The « color field » corresponding to the configuration σ is

$$\mathbf{f}_\sigma = \sum_i (r_i^j - b_i^j)\, \mathbf{c}_j \,, \tag{3}$$

where summation over repeated indices is assumed. The « color flux » of an output configuration s' is

$$\mathbf{q}_{s'} = (r_i - b_i)\, \mathbf{c}_i \,. \tag{4}$$

The configuration that minimizes the product $-\mathbf{f}_\sigma \cdot \mathbf{q}_{s'}$ is chosen. In practice this rule is difficult to implement because of the large number of fields $\mathbf{f}_\sigma$ that can be realized. In appendix A we describe a simplification of that rule which results in the exact definition of the rate $A(s, s', \sigma)$ at which a collision changes s into s' in the presence of a neighbor configuration σ.

Unlike spinodal decomposition in nature, the explanation of the decomposition observed in the ILG lies in the kinetic rather than the equilibrium properties of the system. It seems that at low densities the Boltzmann equation approach is still valid for the gas. Molecular chaos holds in the sense described in [4]. From this assumption it is possible to show how the dynamics make the single mixed phase unstable. Let $d(\mathbf{x}, t)$ be the local reduced density (number of particles divided by 7) and $\theta(\mathbf{x}, t)$ be the local fraction of red particles. The average flux of color can be defined as $\mathbf{J} = \langle \mathbf{q} \rangle$. If the steady state reached with d and θ uniform and constant in time is slightly perturbed, with θ not uniform but d still so, one expects a linear response :

$$\mathbf{J} = -Dd\, \nabla\theta \,. \tag{5}$$

In reversible LGA's, an H theorem holds [12] and one can show that transport coefficients must be positive. On the other hand in the ILG one may obtain $D < 0$. Indeed the color field $\mathbf{f}_\sigma$ is a local estimate of $\nabla(d\theta)$. The collision rule tends to align $\mathbf{J}$ with the color gradient and thus make D negative.

A fundamental understanding of D is thus a crucial component of a fundamental understanding of the ILG. In the following section, we try to estimate D by constructing a Chapman-Enskog solution of the Boltzmann equation. From these estimates of D we may then predict the transition to a two-phase state in a $d - \theta$ diagram.

The Chapman-Enskog estimation of the diffusion coefficient.

In our statistical approach we investigate one-particle distribution functions and call $R_i(\mathbf{x}, t)$ and $B_i(\mathbf{x}, t)$ the probability of having respectively a red or a blue particle at site $\mathbf{x}$ in direction i. As in [4], $N_i = R_i + B_i$ is the probability of finding any particle in direction i. The Boltzmann equation is obtained by a molecular chaos postulate. We assume that the

arriving particles at a site and those at neighboring sites are all independently distributed variables. This assumption is usually rather successful for predicting viscosities [12, 13] and diffusivities [5]. In the present context this is a relatively crude assumption : numerical simulations of the ILG show correlations between the colors observed at neighboring sites. The Boltzmann equation approach is nevertheless useful : it allows an intuitive understanding of the mechanism that leads to the decomposition into two phases. Accordingly the probability of a configuration (s, σ) of a site and its neighbor given a state described by the one-particle densities R_i, B_i can be written as

$$P(s, \sigma) = P(s)\, W(\sigma) \tag{6}$$

where

$$P(s) = \prod_{i=0}^{i=6} R_i^{r_i}(\mathbf{x}, t)\, B_i^{b_i}(\mathbf{x}, t)[1 - N_i(\mathbf{x}, t)]^{1-s_i} \tag{7}$$

and where

$$W(\sigma) = \prod_{j=1}^{6} \prod_{i=0}^{6} R_i^{r_i^j}(\mathbf{x} + \mathbf{c}_j, t)\, B_i^{b_i^j}(\mathbf{x} + \mathbf{c}_j, t)[1 - N_i(\mathbf{x} + \mathbf{c}_j, t)]^{1-s_i^j}. \tag{8}$$

Clearly P and W depend implicitly on the local one-particle densities R_i, B_i. The Boltzmann equation is then

$$R_i(\mathbf{x} + \mathbf{c}_i, t+1) - R_i(\mathbf{x}, t) = \sum_{s, s', \sigma} (r_i' - r_i)\, A(s, s', \sigma)\, W(\sigma)\, P(s) \tag{9}$$

where $A(s, s', \sigma)$ is the probability of an output s' given an input s and an input neighbor configuration σ. A similar equation obtained by exchanging red and blue holds. This equation is solved by an expansion around a state of local equilibrium :

$$R_i = R_i^{(0)} + R_i^{(1)} + \cdots, \quad B_i = B_i^{(0)} + B_i^{(1)} + \cdots \tag{10}$$

where $R_i^{(n)}$ is of order n in gradient. The local equilibrium is extremely simple : one lets the fraction of reds be θ and the reduced density be d. The one-particle densities in that state are :

$$R_i^{(0)} = \theta d\,, \quad B_i^{(0)} = (1 - \theta)\, d\,. \tag{11}$$

At next order in the gradient expansion one expects

$$R_i^{(1)} = \gamma c_{i\alpha}\, \partial_\alpha(\theta d)\,, \quad B_i^{(1)} = -\gamma c_{i\alpha}\, \partial_\alpha(\theta d)\,, \tag{12}$$

where we adopt as usual Greek letters to denote vector components. Correspondingly we shall let $P^{(0)}(s)$ and $W^{(0)}(\sigma)$ signify the distributions obtained by replacing R_i and B_i by their first order expressions in (7), (8).

From the Boltzmann equation (9) one obtains at first order in gradient :

$$c_{i\alpha}\, \partial_\alpha\, R_i^{(0)} = \sum_{s, s' \sigma} (r_i' - r_i)\, A(s, s', \sigma)[\mathfrak{B}_1\, W^{(0)}(\sigma) + (\mathfrak{B}_2 + \mathfrak{B}_3)\, P^{(0)}(s)] \tag{13}$$

(no sommation on i), where :

$$\mathfrak{B}_1 = \frac{\partial P(s)}{\partial R_j(\mathbf{x})} R_j^{(1)}(\mathbf{x}) + \frac{\partial P(s)}{\partial B_j(\mathbf{x})} B_j^{(1)}(\mathbf{x})\,, \tag{14}$$

$$\mathcal{B}_2 = \frac{\partial W(\sigma)}{\partial R_j(\mathbf{x}+\mathbf{c}_k)} [R_j^{(0)}(\mathbf{x}+\mathbf{c}_k) - R_j^{(0)}(\mathbf{x})] + \frac{\partial W(\sigma)}{\partial B_j(\mathbf{x}+\mathbf{c}_k)} [B_j^{(0)}(\mathbf{x}+\mathbf{c}_k) - B_j^{(0)}(\mathbf{x})] , \quad (15)$$

and

$$\mathcal{B}_3 = \frac{\partial W(\sigma)}{\partial R_j(\mathbf{x}+\mathbf{c}_k)} R_j^{(1)}(\mathbf{x}+\mathbf{c}_k) + \frac{\partial W(\sigma)}{\partial B_j(\mathbf{x}+\mathbf{c}_k)} B_j^{(1)}(\mathbf{x}+\mathbf{c}_k) . \quad (16)$$

Using equations (7), (8) and the expressions for the distributions $R^{(0)}$, $R^{(1)}$, etc., it is easy to express $\mathcal{B}_1$ and $\mathcal{B}_2$. $\mathcal{B}_1$ is the usual contribution to the deviation from local equilibrium arising from the Chapman-Enskog expansion at first order. $\mathcal{B}_2$ is specific to the immiscible lattice gas collisions. These collisions produce an additional flux of color towards regions of the same color, by letting the outcome of the collisions depend on the neighbor configuration σ. Finally $\mathcal{B}_3$ indicates the change in the neighbor configurations resulting from the distortion of local equilibrium. This distortion leaves the total number of red (or blue) particles on a neighbor site unchanged and should not affect the color fluxes toward the neighbors. Thus it does not come as a surprise that $\mathcal{B}_3 = 0$. Indeed, $W(\sigma)$ is symmetric in the exchange of directions :

$$\frac{\partial W(\sigma)}{\partial R_i(\mathbf{x}+\mathbf{c}_j)} = \frac{\partial W(\sigma)}{\partial R_{i+3}(\mathbf{x}+\mathbf{c}_j)} ,$$

while $R_{i+3}^{(1)}(\mathbf{y}) = -R_i^{(1)}(\mathbf{y})$. Using these identities one sees that the r.h.s. of (16) cancels. Expanding the derivatives in (14) and (15) and replacing in (13) we obtain

$$c_{i\alpha} = (\gamma \mathcal{A}_{ij}^{(1)} + \mathcal{A}_{ij}^{(2)}) c_{j\alpha} , \quad (17)$$

where $\mathcal{A}_{ij}^{(1)}$ and $\mathcal{A}_{ij}^{(2)}$ in the r.h.s. contain contributions respectively from $\mathcal{B}_1$ and $\mathcal{B}_2$. $\mathcal{A}_{ij}^{(1)}$ is given by

$$\mathcal{A}_{ij}^{(1)} = \sum_{s,s'} (r_i' - r_i) \langle A(s, s', \sigma) \rangle_\sigma \, \theta^{p_r - 1}(1-\theta)^{p_b - 1} \, d^{p-1}(1-d)^{7-p} \, s_j(r_j - \theta) \quad (18)$$

where $p_r = \Sigma_i r_i$, $p_b = \Sigma_i b_i$ and $p = p_r + p_b$. In (18) the brackets $\langle \ \rangle_\sigma$ indicate averaging over σ using the factorized distribution (8) in equilibrium :

$$\langle A(s, s', \sigma) \rangle_\sigma = \sum_\sigma A(s, s', \sigma) \, W^{(0)}(\sigma) . \quad (19)$$

Also,

$$\mathcal{A}_{ij}^{(2)} = \sum_{s,s',\sigma} (r_i' - r_i) \, A(s, s', \sigma) \, P^{(0)}(s) \, s_k^j(r_k^j - \theta) \times$$

$$\times \, \theta^{p_{\sigma r} - 1}(1-\theta)^{p_{\sigma b} - 1} \, d^{p_\sigma - 1}(1-d)^{42 - p_\sigma} , \quad (20)$$

where $p_{\sigma r} = \Sigma_{kj} r_k^j$, $p_{\sigma b} = \Sigma_{kj} b_k^j$ and $p_\sigma = p_{\sigma r} + p_{\sigma b}$. The evolution of the color fraction may now be obtained simply as a consequence of the conservation of red particles. Observe that :

$$\sum_{i=0}^{i=6} R_i(\mathbf{x}+\mathbf{c}_i, t+1) = \sum_{i=0}^{i=6} R_i(\mathbf{x}, t) . \quad (21)$$

The usual scaling for diffusion is $\partial_t = \mathcal{O}(\nabla^2)$. Using this scaling, together with (10), (11), (12)

and (17) one obtains

$$\partial_t \theta = D\nabla^2 \theta$$

where

$$D = -\frac{3}{14} - \frac{3\gamma}{7}. \tag{22}$$

Equations (17), (18), (20), and (22) constitute our theoretical prediction for the diffusivity D of color in the ILG. The first term on the r.h.s. of equation (22) is a « propagation » contribution in the sense of reference [4]. The factors $\mathcal{A}^{(1)}$ and $\mathcal{A}^{(2)}$ are polynomials of the 48th degree in d and θ. Although it is in principle possible to compute all the coefficients involved, at this stage we simply performed a numerical calculation of γ for some selected values of d and θ. The details of this numerical computation are presented in appendix B. The results are presented and compared with direct computations from numerical simulations in the next section.

Before illustrating our results, it is interesting to consider the meaning of the various terms in D. The diffusivity calculated above can be broken into two contributions. The first contribution arises if one sets $\mathcal{A}_{ij}^{(2)} = 0$ in (17). The resulting diffusivity D_1 is identical to the self-diffusion coefficient in an equivalent lattice gas, without nearest neighbor interactions but with transition rates given by $\langle A(s, s', \sigma)\rangle_\sigma$. These rates depend on the parameters d, θ through the distribution of neighbor configurations in equilibrium, $W(\sigma\,; d, \theta)$, as shown by equation (19). Numerical calculations have always shown that D_1 was positive. It seems likely that this would always be the case. But we have found no rigorous way to determine the sign of D_1. In particular, the averaged rates do not verify semi-detailed balance. Thus the method employed in [12] cannot be used. Semi-detailed balance does not hold because even when the neighbor color field is 0 on average, certain output configurations get selected more often as they are optimal for the instantaneous color field.

The second contribution to D comes from the term $\mathcal{A}_{ij}^{(2)}$: it represents the effect of a gradient of concentration on the distribution of the neighboring sites. This contribution is always negative.

Comparisons of theoretical and empirical estimates of *D*.

To assess the accuracy of our theoretical estimate of D, we have performed two independent numerical experiments. The first is a direct comparison of the predicted values of D with measurements of D made from simulations. In the second experiment we compare the spinodal curve obtained from the predicted zeroes of D with results obtained from numerical domain-growth experiments.

EMPIRICAL ESTIMATE OF THE DIFFUSION COEFFICIENT. — Empirical estimates of the diffusion coefficient were obtained by performing simulations in square boxes with the density set at d and the color fraction set at $\theta + a$ on one side and $\theta - a$ on the other. Boxes of various sizes L (11×11, 20×20 and 27×27) were used.

This experiment requires somewhat more care than analogous experiments performed with the simplest possible LGA mixtures [5]. Of particular interest is the way we set the color fraction at the boundaries. Specifically, two additional columns of nodes are used on each side. Nodes are reset at each time step to the desired color fraction and density by regenerating sites randomly with the expected distribution of red, blue, and empty cells. The random generation is done after the propagation step of the lattice gas and before the

collisions. At least two additional columns are necessary, because the outcome of the collisions in the second column will depend on the color in the first column.

To obtain D, we first measure the flux $\mathbf{J}$ of color by counting the number of red or blue particles crossing a vertical line. The diffusion coefficient is best expressed in terms of a « conductivity » $\kappa(d, \theta) = dD(\theta, d)$. We estimate it by

$$\kappa = \frac{JL}{2a}. \tag{23}$$

The theoretical predictions for this quantity as well as the measured results are shown in figure 4 for $\theta = 0.5$, $0.02 \leqslant d \leqslant 0.28$. We repeated these experiments for $\theta = 0.75$ with similar results.

Statistical errors are estimated by repeating the experiment about 30 times and estimating the standard deviation. There are several sources of statistical error. The most important is related to averaging over noisy time series for the color flux. If fluxes were uncorrelated from one time to the next the error would be of order $N^{-1/2}$, where N is the total number of red and blue particles crossing the measuring line. At low density very few particles are observed and this statistical error increases. This explains the large error bar on the left-hand-side of figure 4. The measurement is also affected by long-range, large-time correlations near the critical point. Physically these correlations correspond to the presence of blobs of blue or red phases, which persist for a typical time τ_0 and have a typical size ξ_0. Because of these correlations one must average over times much longer than τ_0. The presence of these correlations is responsible for the large error bars near the critical point in figure 4.

The agreement is good between theory and numerical experiment near $d = 0$. This is not surprising since one expects the Boltzmann equation to be approximately valid when the neighboring nodes are weakly coupled. The theoretical and numerical values are in disagreement away from $d = 0$, but the transition point is not too far from the predicted value : 0.23 ± 0.02 from experiment *versus* 0.20 from theory.

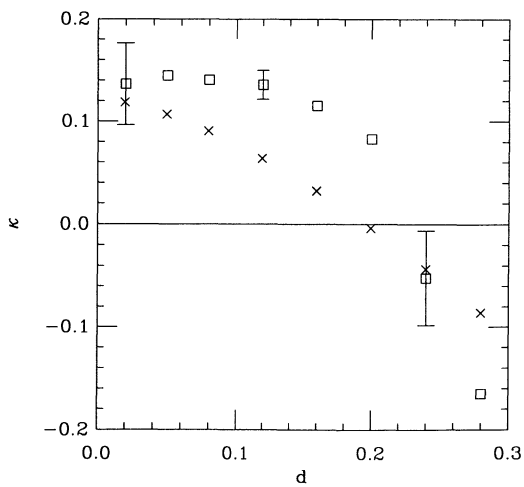

Fig. 4. — Plot of the theoretical and numerical values of the diffusion coefficient κ defined in the text. Squares represent numerical-experimental values and (×)'s represent theoretical values. Typical error bars are plotted, representing two standard deviations.

EMPIRICAL DETERMINATION OF THE SPINODAL CURVE. — If $D > 0$, a mixed state (equal concentrations of both colors) is stable. $D < 0$, on the other hand, implies instability : an infinitesimal perturbation of sufficient wavelength should result in decomposition into two phases. The locus of points for which $D = 0$ as a function of d and θ is therefore the spinodal curve for the ILG.

Numerical solutions of equations (17), (18), (20), and (22) for $D(d, \theta) = 0$ are depicted in figure 7 as small squares. To compare this approximate prediction with results from simulation we could simply repeat the diffusivity experiments described above for a variety of values of d and θ. We have chosen, however, a different route that makes specific contact with our study of phase transitions : measurements of the growth rate of the correlation length. We assume that the correlation length $\xi(t) \propto t^{\alpha}$, where t is the number of time steps and the exponent $\alpha \geqslant 0$ for simulations initialized as homogeneous mixtures. We may thus estimate the location of the spinodal curve by determining the limiting values of d and θ which yield positive α.

We performed experiments with boxes of size 32×32, initialized as random mixtures for various values of d and θ. Correlation lengths were estimated at discrete intervals of time by 2-D Fourier transformation of the relative color density

$$\rho_c(\mathbf{x}, t) = \sum_i [r_i(\mathbf{x}, t) - b_i(\mathbf{x}, t)] , \tag{24}$$

where the sum is taken over the 7 possible velocities and $\mathbf{x}$ is a discrete position vector. By assuming isotropy of the ILG (confirmed qualitatively by inspection), we work with the circularly averaged modulus of the 2-D transform of ρ_c, given by

$$\hat{\rho}_c(k, t) = \left\langle \left| \sum_{\mathbf{x}} e^{-i\mathbf{k}\cdot\mathbf{x}} \rho_c(\mathbf{x}, t) \right| \right\rangle , \tag{25}$$

where the discrete wavenumber $k = |\mathbf{k}|$ and the brackets denote circular averaging. The correlation length is defined to be proportional to the inverse of the $\hat{\rho}_c$-weighted average of k :

$$\xi(t) \propto \frac{\sum_k \hat{\rho}_c(k, t)}{\sum_k k\hat{\rho}_c(k, t)} . \tag{26}$$

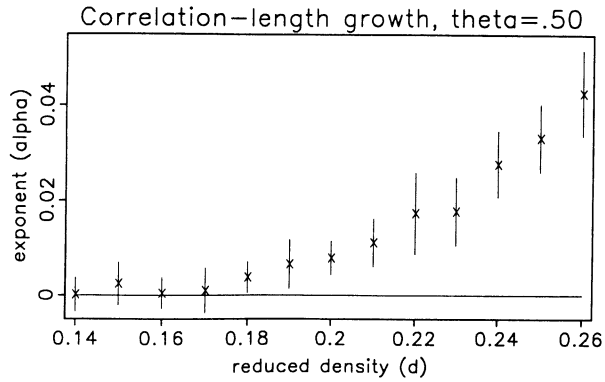

Fig. 5. — Plot of the growth exponent, α, for varying d at fixed $\theta = 0.5$. Error bars represent two standard deviations. Based on these data, the transition density is taken to be $d \approx 0.19$.

For each $d - \theta$ pair, the ILG was run 12 times with different initial conditions for 1 000 time steps. The growth exponent α was then estimated for each run by measuring the slope in a log-log plot of $\xi(t)$. Typical results are shown in figures 5 and 6. In figure 5, d varies while the concentration is fixed at $\theta = 0.50$, whereas in figure 6, θ varies while the reduced density is fixed at $d = 0.30$. Each point represents the mean of α, for the 12 independent runs ; the error bars represent 2 standard deviations from the mean. The error bars are relatively small when $\alpha \approx 0$ because $\xi(t)$ is approximately flat for each run. The larger error bars that occur for positive α have two causes. One cause is hysteresis near the critical point : growth may begin at different times in each simulation. The second source of error is our assumption of the power law for the growth of ξ, which has of yet no firm foundation. Finite-size affects appear insignificant : similar tests for boxes of twice the size yielded similar results.

We determine points (d, θ) on the spinodal curve by identifying by eye the value of d (or θ) at which $\alpha(d)$ (or $\alpha(\theta)$) departs from the line $\alpha = 0$. For the data of figure 5, we

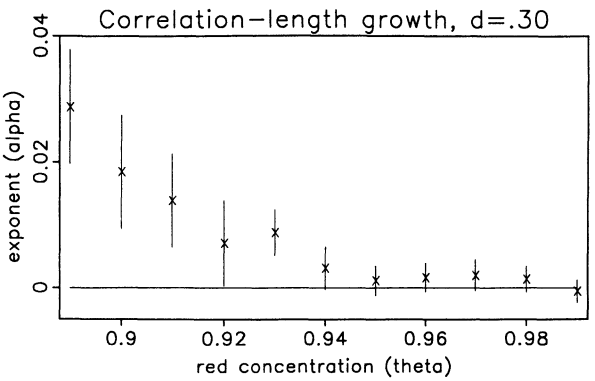

Fig. 6. — Plot of the growth exponent, α, for varying θ at fixed $d = 0.3$. Error bars represent two standard deviations. Based on these data, the transition concentration is taken to be $\theta \approx 0.93$.

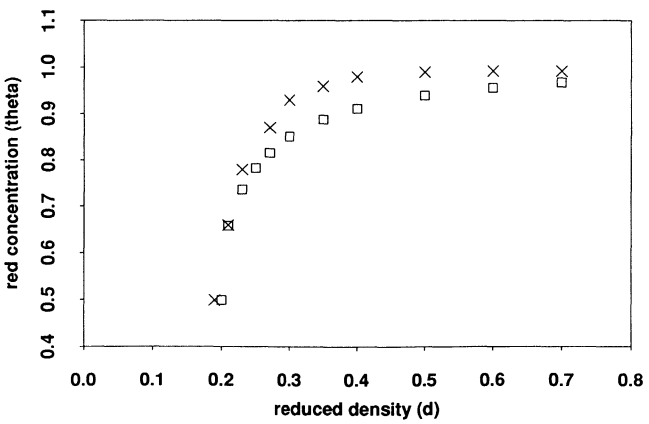

Fig. 7. — Phase diagram of the immiscible lattice gas. Squares represent the theoretical predictions for $D(d, \theta) = 0$, (×)'s represent observations from simulations. Errors in the observations are approximately the same size as the symbols. Locations inside the curve formed by the empirical points represent regions of stable decomposition of the two phases.

find $d_c = 0.19$; similarly, for the data of figure 6, $\theta = 0.93$ at the transition. We consider the errors in these estimates to be on the order of ± 0.02. We note that the value of d_c obtained in our diffusion and domain growth experiments differ but the discrepancy falls within the error bars.

By performing the same measurements at different locations in the space of d and θ, we obtained the empirical spinodal curve in figure 7. These estimates are compared to the theoretical predictions of $D(d, \theta) = 0$. Experiment and theory compare reasonably well. As in the direct numerical estimates of D, we interpret the deviations from the theoretical predictions primarily as a limitation of the Boltzmann approximation for the ILG.

Conclusions.

We have introduced a jointly theoretical and empirical approach to the study of spinodal decomposition in immiscible lattice gases. We have shown that phase separation occurs in ILG's not because of a favorable free energy (no such quantity appears to exist) but rather because of its unusual kinetic properties. Specifically, for certain combinations of density and concentration, the diffusion coefficient of the ILG becomes negative, providing for the decomposition of phases. Theoretical predictions based on the Boltzmann approximation and empirical studies of diffusion and domain growth have each confirmed the existence of a phase diagram in the plane of density and concentration for the ILG. The resulting spinodal curve separates the region where a single phase can be stable from the region where it decomposes into domains containing both phases. The agreement between the predictions derived from the molecular chaos assumption and the empirical observations is qualitatively good.

There are several consequences to this description. One is that it is unlikely that more stable phases would be discovered in this model than are already known. However, the precise nature of the behavior in the region between $d \simeq 0.2$, at the critical point of the phase diagram, and $d \simeq 0.4$, where the surface tension measured in reference [6] vanishes, is not clear. One possibility is that the surface tension was too small to be observed in this region by the methods of reference [6], but this conjecture will have to be clarified by further analysis. Another point that requires some clarification is the effect of dilution on the behavior of the immiscible phases. Transport properties such as viscosity and diffusion rate in the stable phases should be investigated. Finally, we note that we have only scratched the surface of the most important of our objectives — the precise delineation of the relationship of the ILG to the classical mixture models of statistical mechanics and hydrodynamics.

Acknowledgments.

We thank D. d'Humières for interesting discussions. DHR is grateful to the Laboratoire de Physique Statistique, CNRS, for financial support and hospitality during visits. This work was additionally supported in part by NSF Grant EAR-8817027 (DHR) and by the sponsors of the MIT Porous Flow Project.

Appendix A.

The rule that was used differs slightly from the simplified description given in the introduction. The essential effect of maximizing the product $\mathbf{f}_\sigma \cdot \mathbf{q}_{s'}$ is to align the field with the flux. Hence it is only necessary to keep information about the orientation of $\mathbf{f}$. Let $\psi_\sigma = (\mathbf{f}_\sigma, \hat{x})$ be the angle of the field with the x axis. The exact field $\mathbf{f}_\sigma$ is replaced by a field $\mathbf{f}'_{k_\sigma}$, where $\mathbf{f}'_k = (\cos 2\pi k/N, \sin 2\pi k/N)$ and k_σ is a number between 0 and $N-1$ that

verifies

$$2\pi(k_\sigma - 1/2)/N < \psi_\sigma \leqslant 2\pi(k_\sigma + 1/2)/N . \tag{27}$$

When $\mathbf{f}$ is zero $\mathbf{f}' = \mathbf{f}'_N$ is also zero. Then the product $\mathbf{f}'_{k_\sigma} \cdot \mathbf{q}_{s'}$ is maximized. Higher values of N yield better approximations of the true field. Since the interface is fluctuating it is likely that a very accurate approximation would be unnecessary. In this paper all calculations were made with $N = 36$.

For each input configuration s there is a class of output configurations $\mathcal{C}_s$ which share the same values of momentum and have the same number of red and blue particles. Among all those only a subset maximize $\mathbf{f}'_{k_\sigma} \cdot \mathbf{q}_{s'}$. Let $\mathcal{C}_{s,\sigma}$ be that subset. For instance if $\mathbf{f} = 0$ then $\mathcal{C}_{s,\sigma} = \mathcal{C}_s$. One choses randomly between the configurations in $\mathcal{C}_{s,\sigma}$ using a random number generator. This implies a transition rate given by

$$A(s, s', \sigma) = \begin{cases} [\mathcal{C}_{s,\sigma}]^{-1} & \text{if } s' \in \mathcal{C}_{s,\sigma} \\ 0 & \text{otherwise} . \end{cases} \tag{28}$$

where $[\mathcal{C}]$ denotes the number of elements in set $\mathcal{C}$. Since the transition rate depends on σ only through k_σ one may define $A'(s, s', k)$ to be the rate of transition in presence of a color field indexed by $k = k_\sigma$.

Appendix B.

The computation of $\mathcal{A}^{(2)}$ is the most lengthy. It involves summing over 3^{42} neighbor configurations. This can be simplified by rewriting (20) in the following way

$$\mathcal{A}^{(2)}_{ij} = \sum_{s, s', k} (r'_i - r_i) A'(s, s', k) P^{(0)}(s) W_j(k) \tag{29}$$

where

$$W_j(k) = \sum_{\sigma : k_\sigma = k} s^j_\ell (r^j_\ell - \theta) \theta^{p_{\sigma r} - 1} (1 - \theta)^{p_{\sigma b} - 1} d^{p_\sigma - 1} (1 - d)^{42 - p_\sigma} . \tag{30}$$

The computation of $W_j(k)$ may be further simplified by factorizing the contributions of the 6 nearest neighbors in the above sum.

References

[1] GUNTON J. D., SAN MIGUEL M. and SAHNI P. S., Phase Transitions and Critical Phenomena, eds. C. Domb and J. L. Leibowitz (Academic Press) 1983.

[2] ROWLINSON J. S. and WIDOM B., Molecular Theory of Capillarity (Clarendon Press, Oxford) 1982.

[3] FRISCH U., HASSLACHER B. and POMEAU Y., *Phys. Rev. Lett.* **56** (1986) 1505.

[4] FRISCH U., D'HUMIÈRES D., HASSLACHER B., LALLEMAND P., POMEAU Y. and RIVET J.-P., *Complex Syst.* **1** (1987) 648.

[5] BURGES C. and ZALESKI S., *Complex Syst.* **1** (1987) 31.

[6] ROTHMAN D. H. and KELLER J. M., *J. Stat. Phys.* **52** (1988) 1119.

[7] BOGHOSIAN B., TAYLOR W. and ROTHMAN D. H., A cellular-automata simulation of two-phase flow on the CM-2 Connection Machine computer, to appear in Proceedings of Supercomputing '88 (sponsored by IEEE and ACM-SIGARCH) 1988.

[8] ZANETTI G., The hydrodynamics of the lattice gas, U. Chicago preprint, to be published (1988).
[9] WOLFRAM S., *J. Stat. Phys.* **45** (1986) 471.
[10] ROTHMAN D. H., Lattice-gas automata for immiscible two-phase flow, to appear in Discrete Kinetic Theory, Lattice-Gas Dynamics, and Foundations of Hydrodynamics, Ed. R. Monaco (World Scientific, Singapore) 1989.
[11] LANDAU L. D. and LIFSHITZ E. M., Statistical Physics, 3rd ed. (Pergamon Press, New York) 1980.
[12] HÉNON M., *Complex Syst.* **1** (1987) 762.
[13] D'HUMIÈRES D. and LALLEMAND P., *Complex Syst.* **1** (1987) 598.